INORGANIC CHEMISTRY FRONTIERS

RESEARCH ARTICLE

View Article Online
View Journal | View Issue

Cite this: *Inorg. Chem. Front.*, 2024, **11**, 2039

Chiral lanthanide hexaazamacrocycles for circularly polarized luminescence, high relaxivity and magnetic resonance imaging†

Yuxin Tang,[a] Minghong Jian,[c] Baobing Tang,[b] Zhenhua Zhu,[d] Zhenxin Wang[c] and Yunling Liu *[b]

Multifunctional lanthanide complexes have been extensively studied in recent years owing to their widespread applications in physics, chemistry and biology, including quantum information processing, molecular spintronics and theranostics. The multifunctionality includes chirality, luminescence, magnetism, ferroelectricity, fluorescence/magnetic resonance imaging *etc*. Although various N- and O-donor ligands have shown the ability to synthesize these complexes, Schiff bases are still the most widely used in constructing air-stable species. Herein, we report the facile gram-level synthesis of three pairs of lanthanide macrocycle enantiomers *via* an *in situ* [2 + 2] imine condensation with a trivalent lanthanide ion as a template. Eu(III)-based compounds, ***R*/*S*-Eu** and ***R*/*S*-Eu-Ph$_3$PO**, both show efficient circularly polarized luminescence (CPL) with maximum dissymmetry factors (g_{lum}) of 0.098 and 0.110, respectively. The latter exhibited stronger emission intensity and a longer luminescence lifetime than the former due to the lower vibrational coordination structures around the Eu(III) ion. Gd(III)-based species, ***R*/*S*-Gd**, possess a relatively high relaxivity of up to 35.04 and 34.09 mM^{-1} s^{-1} for *R*- and *S*-enantiomers, benefitting from the presence of one coordinated water molecule and abundant intermolecular H-bonds. In addition, the results of the MTT assay and *in vitro* experiments demonstrated the low toxicity and efficient MRI of Gd(III)-chelates in A549 cells.

Received 29th January 2024,
Accepted 23rd February 2024

DOI: 10.1039/d4qi00275j

rsc.li/frontiers-inorganic

Introduction

Lanthanide macrocyclic compounds have exhibited versatile applications across various fields, including display devices, information storage, magnetic resonance imaging (MRI) and molecular theranostics by virtue of their excellent luminescence properties, enormous magnetic anisotropy, high thermostability/air-stability and facile modification.[1–5] They can be mainly divided into the following families according to the type of organic ligand (Fig. 1): DOTA derivates,[6] porphyrin,[7,8] phthalocyanine,[9] crown ether,[10] Schiff-base,[11] metallacrown[12]

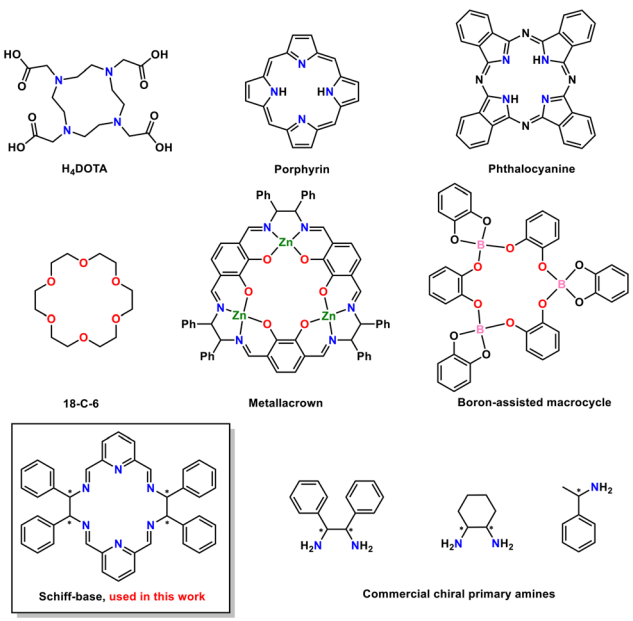

Fig. 1 Representative macrocyclic ligands for lanthanide ions and commercially available chiral primary amines.

[a]*School of Life Sciences, Jilin University, Changchun 130012, P. R. China*
[b]*State Key Laboratory of Inorganic Synthesis and Preparative Chemistry, College of Chemistry, Jilin University, Changchun 130012, P. R. China. E-mail: yunling@jlu.edu.cn*
[c]*State Key Laboratory of Electroanalytical Chemistry, Changchun Institute of Applied Chemistry, Chinese Academy of Sciences, Changchun 130022, P. R. China*
[d]*State Key Laboratory of Rare Earth Resource Utilization, Changchun Institute of Applied Chemistry, Chinese Academy of Sciences, Changchun 130022, P. R. China*

†Electronic supplementary information (ESI) available: Crystallographic data, quantum yield, magnetic characterization *etc*. CCDC 2313857 (***S*-Eu**), 2313859 (***R*-Eu**), 2313860 (***R*-Gd**), 2313872 (***S*-Gd**) 2326392 (***R*-Eu-Ph$_3$PO**), 2326394 (***S*-Eu-Ph$_3$PO**) and 2328816 (***R*-Y**). For ESI and crystallographic data in CIF or other electronic format see DOI: https://doi.org/10.1039/d4qi00275j

and heteroatom-assisted macrocycles.[13] Among them, Schiff-base lanthanide macrocycles are probably the easiest to obtain *via* a metal-template reaction between a primary amine and a carbonyl. In particular, the commercially available chiral primary amines, *e.g.* (1*R*,2*R*)-1,2-diphenylethylenediamine, (1*R*,2*R*)-1,2-diaminocyclohexane and (*R*)-1-phenylethan-1-amine (Fig. 1), facilitate the construction of multifunctional lanthanide compounds.[14,15] Comparatively, chiral DOTA,[16] porphyrin[17] and phthalocyanine[18] usually involve more complicated synthesis and purification. In addition, Schiff-base macrocycles offer a simpler method to construct multiple-decker lanthanide sandwich complexes for magnetic interaction studies compared to phthalocyanine derivates.[19,20]

For circularly polarized luminescence (CPL), chiral lanthanide compounds with suitable sensitizing ligands usually exhibit a much higher dissymmetry factor (g_{lum}) than organic molecules by virtue of most magnetically allowed f–f transitions,[21] which expands the application of lanthanide probes with CPL detection to biological assays.[22] Recently, a more comprehensive evaluating tool, *i.e.* CPL brightness (B_{CPL}), involving two additional parameters, absorption extinction coefficient, ε and quantum yield, φ, besides g_{lum}, was proposed to quantify the performance of CPL emitters.[23] Among all chiral lanthanide compounds, Eu(III)-based compounds are the most studied giving the largest g_{lum} value to date, up to 1.38.[24] One of the most efficient strategies to enhance CPL activity is increasing the rigidity of the complex,[25] *e.g.* the recently reported heterobimetallic binolate Er(III) complex[26] and spinolate Tb(III) complex.[27] In addition, substituents, auxiliary ligands and external stimuli can also influence CPL properties, which has been clearly demonstrated by a series of enantiopure Eu(III) macrocycle complexes.[28] Both the chiral substituents on the macrocycle scaffolds and external static magnetic fields enabled an evident increase in g_{lum}. It is worth noting that apart from improving CPL performance, some macrocyclic ligands, *e.g.* DOTA derivates, also enable the exceptional water solubility of complexes, which is advantageous for their biological applications.

In terms of the size of the macrocycle cavity, penta- and hexa-azamacrocycles exhibited the ability to encapsulate trivalent lanthanide ions in the equatorial plane, giving rise to complexes with high symmetry.[11,29] Recently, such lanthanide macrocycles have received increasing attention in the field of single-molecule magnets (SMMs), making some impressive achievements,[30] *e.g.* the current record-holder of the anisotropy barrier for air-stable SMMs, *RRRR*/*SSSS*-Dy-$D_{6h}F_{12}$.[31] In 2022, Shanmugam *et al.* reported a discrete bifunctional macrocyclic Schiff-base Ce(III) complex that combines ferroelectricity with field-induced SMM behavior.[32] It is noteworthy that such encapsulations can also prevent the proximity of high-energy oscillators to lanthanide ions to some extent, therefore enhancing the luminescence properties.[33] In addition, since the Gd-DOTA compound was clinically approved as a contrast agent for human use in 1989, macrocyclic Gd(III) chelates have been greatly studied in the MRI contrast agent field due to their improved safety (more kinetically inert than acyclic species) and satisfactory relaxivity.[2] From a molecular structural point of view, excellent luminescence properties and high relaxivity seem to be contradictory as the latter usually needs inner-sphere coordinated water (*vide infra*) while the former does not, with the presence of an O–H oscillator accelerating the non-radiative quenching pathways. Herein, we report the one-pot synthesis of lanthanide hexaazamacrocycle enantiomers, $[Ln(L^{N6})Cl_2CH_3OH][Ln(L^{N6})Cl_2H_2O]Cl_2$ (Ln = Eu and Gd, L^{N6} is the chiral Schiff-base macrocycle derived from the imine condensation between 2,6-diformylpyridine and (1*R*,2*R*)/(1*S*,2*S*)-1,2-diphenylethylenediamine; ***R*/*S*-Eu** and ***R*/*S*-Gd**). Eu(III) complexes show strong chiroptical properties ($|g_{lum}|$ = 0.1, B_{CPL} = 71.45 M^{-1} cm^{-1}), while Gd(III) analogues possess relatively high relaxivity up to 35.04 and 34.09 mM^{-1} s^{-1} for the *R*- and *S*-enantiomer, respectively, and exhibit efficient MRI at low concentrations. In addition, another pair of Eu(III) enantiomers, $[Eu(L^{N6})(Ph_3PO)_2(ClO_4)][ClO_4]_2$ (***R*/*S*-Eu-Ph$_3$PO**), with the same equatorial macrocycle as ***R*/*S*-Eu**, was also prepared, showing enhanced luminescence and chiroptical properties by virtue of lower-vibrational coordination structures around Eu(III) ions. To the best of our knowledge, this is the first study of chiral hexaazamacrocycles that support both strong circularly polarized luminescence (CPL) and high relaxivity as well as *in vitro* MRI.

Experimental

Chemicals and synthesis

$EuCl_3·6H_2O$, $GdCl_3·6H_2O$, (1*R*,2*R*)-1,2-diphenylethylenediamine and (1*S*,2*S*)-1,2-diphenylethylenediamine were purchased from Sigma-Aldrich. 2,6-Diformylpyridine was synthesized as reported previously.[34] All solvents were commercially available and used as received without any further purification. All experiments were performed under aerobic conditions. ***R*/*S*-Eu** and ***R*/*S*-Gd** were synthesized by the following procedure: $LnCl_3·6H_2O$ (4 mmol) was dissolved in 80 ml of CH_3OH at room temperature and then homochiral diphenylethylenediamine (8 mmol) and 2,6-diformylpyridine (8 mmol) were added. The mixture was heated under reflux for 8 h. After cooling to room temperature, the solvent was removed on a rotary evaporator, affording the target compound as a white solid in quantitative yield. The single crystals suitable for X-ray measurement can be obtained by the slow diffusion of Et_2O into CH_3OH solution at room temperature for several days. ***R*/*S*-Eu-Ph$_3$PO** was prepared by two steps: firstly, the precursor was synthesized using a similar method to ***R*/*S*-Eu** except that $Eu(ClO_4)_3·6H_2O$ was used; then, 1 mmol (*ca.* 1.07 g) precursor and 2 mmol Ph_3PO (0.56 g) were dissolved in 25 ml of CH_3OH and then heated at 65 °C for 10 h. After that, the system was allowed to cool to room temperature within 24 h, giving light yellow crystals at the bottom of the vial (yield: 51% based Eu).

Instruments and measurements

Single-crystal X-ray data for ***R*/*S*-Ln** and ***R*/*S*-Eu-Ph$_3$PO** were collected at 180 K on a Bruker SMART APEX diffractometer

(Bruker AXS, Ettlingen, Germany) equipped with graphite-monochromatized Mo Kα radiation (λ = 0.71073 Å). The structures were solved and refined in Olex2 by intrinsic phasing (SHELXT) and full-matrix least-squares on F^2 (SHELXL), respectively.[35–37] All non-hydrogen atoms were refined with anisotropic thermal parameters. All hydrogen atom positions were calculated geometrically and refined using the riding model. The crystal data have been deposited at the Cambridge Structural Database (CCDC 2313857, 2313859, 2313860, 2313872, 2326392, 2326394, and 2328816†). UV-vis spectra were recorded in moderate rate mode on a SHIMADZU UV-1750 UV-vis spectrophotometer. The photoluminescence excitation and emission spectra and luminescence decay lifetimes were collected on an Edinburgh FLSP-920 at room temperature. The overall luminescence quantum yields were determined using an integrating sphere on a fluorescence spectrophotometer (C9920-2, Hamamatsu Photonics K. K., Japan). CPL and total luminescence measurements were performed on a JASCO CPL-300 with a bandpass of 10 nm. The ^{1}H-NMR and ^{13}C-NMR spectra were recorded at 500 and 126 MHz, respectively, on a Bruker AV. Chemical shifts are given relative to TMS. High-resolution mass spectra (HRMS) were obtained on an IonSpec Ultima 7.0 T FT-ICR-MS (IonSpec, USA) using ESI and MALDI as an ionization method. The static magnetic properties were explored by variable-temperature direct current (dc) magnetic susceptibility measurement in the temperature range of 1.9–300 K and under a 1000 Oe dc field on a Quantum Design MPMS XL-7 SQUID magnetometer. Thermogravimetric analysis (TGA) spectra were recorded on a NETZSCH STA 449F5 instrument in the range of 30–800 °C at a heating rate of 10 K min^{-1} under N_2 conditions. The relaxation rates of ***R*/*S*-Gd** aqueous solutions with different concentrations were determined on a 1.2 T MRI scanner (Shanghai, China). The cytotoxicity of gadodiamide hydrate and ***R*/*S*-Gd** was assessed using a conventional 3-(4,5-dimethylthiazol-2-yl)-2,5-diphenyltetrazolium bromide (MTT) assay. Briefly, the lung cancer cells (A549 cells) were seeded at 10 000 cells per well in a 96-well plate and cultured in Dulbecco's modified Eagle's medium (DMEM) supplemented with 10% fetal bovine serum (FBS) and 100 U mL^{-1} penicillin–streptomycin for 24 h. After washing with PBS three times, the fresh culture medium containing various concentrations of gadodiamide hydrate and ***R*/*S*-Gd** was added to the cells and continually incubated for 24 h. Finally, the cells were washed with PBS three times and cultured in 100 μL of fresh medium containing 10 μL of 0.5 mg mL^{-1} MTT. After 4 h of incubation, the supernatant was replaced with 100 μL of dimethyl sulfoxide (DMSO) and shaken for 10 min. The optical intensity (OD) at 490 nm was read using a PowerWave XS2 microplate reader. The untreated cells served as the control samples, and the cell viability was calculated by dividing the OD of drug-treated samples by the OD of control samples. For *in vitro* T_1-weighted MRI studies, A549 cells were seeded in a 6-well plate for 24 h and incubated with various concentrations of gadodiamide hydrate and ***R*/*S*-Gd** for another 24 h. After being washed with PBS three times, the cells were detached using trypsin and concentrated *via* centrifugation (1000 rpm, 5 min). The cells were immobilized using 1% agarose for MRI testing.

Results and discussion

Syntheses, crystal structures and magnetism

***R*/*S*-Ln** were *in situ* synthesized *via* a [2 + 2] imine condensation reaction between (1*R*,2*R*)/(1*S*,2*S*)-1,2-diphenylethylenediamine and 2,6-diformylpyridine with $LnCl_3{\cdot}6H_2O$ (Ln = Eu, Gd) as a template in CH_3OH at 65 °C, while ***R*/*S*-Eu-Ph$_3$PO** were prepared using two steps: (i) Eu(III)-macrocycle precursors were synthesized using $Eu(ClO_4)_3{\cdot}6H_2O$ as a template; (ii) the coordinated solvent molecules at the axial positions in the precursors were replaced by Ph_3PO (Scheme 1). The crystalline samples suitable for single-crystal X-ray diffraction (SCXRD) were obtained by slow vapor diffusion and slow cooling approaches for ***R*/*S*-Ln** and ***R*/*S*-Eu-Ph$_3$PO**, respectively. The SCXRD structural analysis suggested that ***R*/*S*-Ln** and ***R*/*S*-Eu-Ph$_3$PO** crystallized in the chiral polar space group, $P2_1$, and the chiral non-polar space group, $P2_12_12_1$, respectively (Tables S1–S3†). The asymmetric unit of ***R*/*S*-Ln** contains two independent cationic lanthanide macrocycles while for ***R*/*S*-Eu-Ph$_3$PO**, only one cationic Eu(III) macrocycle, $[Eu(L^{N6})(Ph_3PO)_2(ClO_4)]^{2+}$, was observed. As shown in Fig. 2, Eu(III) and Gd(III) ions are both nine-coordinate and encapsulated in the Schiff-base macrocycle, giving a hula-hoop local coordination geometry determined by continuous shape measurement (Tables S11–S13†). Therefore, all complexes have the same equatorial ligand, but for axial positions, they are occupied by two chlorides and one H_2O or CH_3OH molecule for ***R*/*S*-Ln** and three oxygen atoms from two Ph_3PO and one ClO_4^- for ***R*/*S*-Eu-Ph$_3$PO**, respectively. Given that enantiomeric lanthanide complexes generally show little difference in the first coordination environment, here, we only described the structural characteristics of ***S*-Ln** and ***S*-Eu-Ph$_3$PO**. The important structural parameters of these six compounds can be found in Tables S5–S10.† For ***S*-Eu**, the average Eu–N bond length is respectively 2.623 and 2.620 Å for Eu1 and Eu2. The Eu–Cl distances are 2.725(3) and 2.678(3) Å for Eu1 and 2.686(3) and 2.716(3) Å for Eu2, respectively. The axial Cl–Eu–Cl bond angles for Eu1 and Eu2 are similar, with a difference of < 3° (Table S8†). It is evident that the largest difference in the coordination environment between Eu1 and Eu2 is the axially coordinated oxygen atoms which come from H_2O and CH_3OH molecules with Eu–O distances of 2.434(6) and 2.518(7) Å, respectively. The Eu1···Eu2 distance is found to be 10.862 Å. We found that ***S*-Eu-Ph$_3$PO** possesses slightly longer Eu–N bond lengths, averaged at 2.630 Å, compared to ***S*-Eu**, suggesting that the replacement of axial ligands can also influence the equatorial crystal field. The average Dy–O distance from Ph_3PO, 2.309 Å, is shorter than the length of Dy–$O_{ClO_4^-}$ of 2.469 Å, due to the strong affinity of Ph_3PO to lanthanide ions, which has also been demonstrated by other luminescent lanthanide compounds with Ph_3PO as the antenna.[33,38] The axial O_{Ph_3PO}–Dy–O_{Ph_3PO} angle is 145.27°, which is comparable to Cl–Eu–Cl angles in ***S*-Eu**. For ***S*-Gd**,

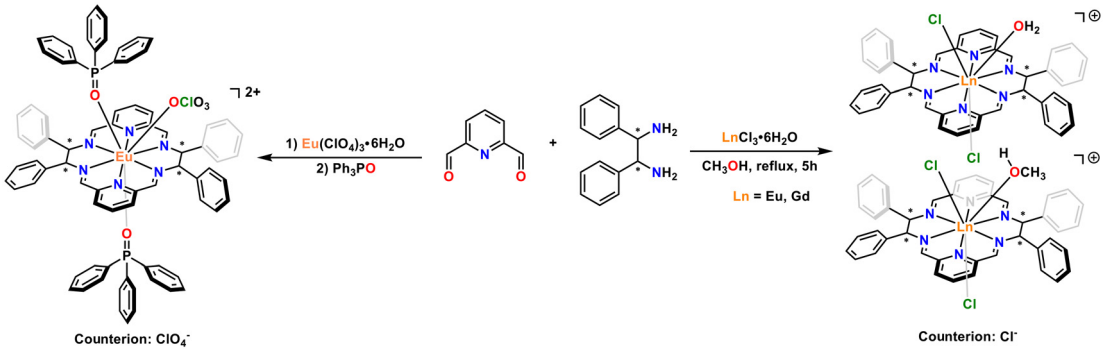

Scheme 1 Synthetic route of ***R*/*S*-Ln** (Ln = Eu and Gd) and ***R*/*S*-Eu-Ph$_3$PO**.

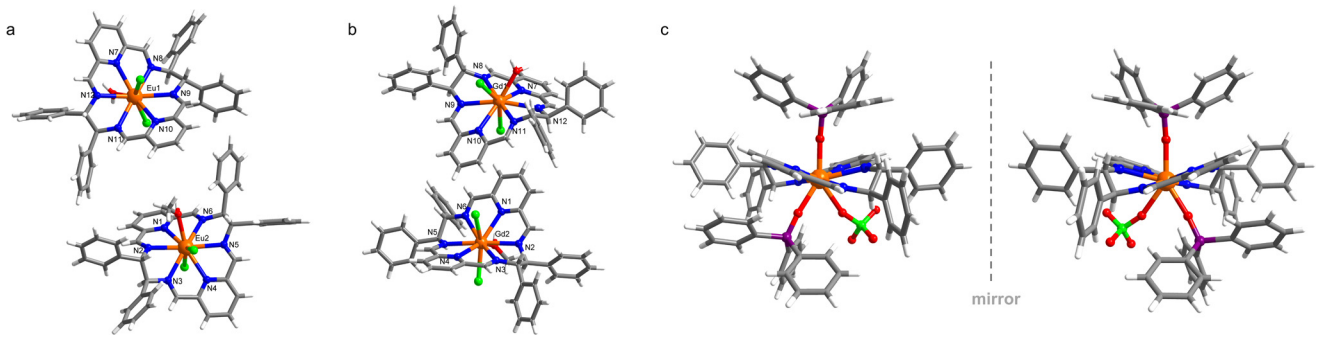

Fig. 2 The ball-and-stick representation of the crystal structures of ***S*-Eu** (a), ***S*-Gd** (b) and ***R*/*S*-Eu-Ph$_3$PO** (c). Color code: orange, Dy; red, O; blue, N; green, Cl; purple, P; white, H.

axial Gd–Cl distances are very similar for Gd1 and Gd2, averaging 2.690 and 2.691 Å, respectively. The equatorial Dy–N bond lengths range from 2.578(6) to 2.679(6) Å for Gd1 and 2.571(7) to 2.688(6) Å for Gd2. The axial Gd–O distances, 2.416(5) Å for Gd1–O_{H_2O} and 2.501(6) Å for Gd2–O_{CH_3OH}, are little shorter than those for ***S*-Eu**. The Gd1···Gd2 distance is 9.669 Å, which is obviously shorter than that of Eu1···Eu2. In addition, the molecular packing of the complexes revealed the presence of abundant hydrogen bonds in the lattice, which is beneficial for relaxivity and luminescence (*vide infra*, Fig. S1†). The static magnetic properties of ***R*/*S*-Gd** were determined (Fig. S2 and S3†), giving the respective $\chi_M T$ values at 300 K of 15.41 and 15.20 cm^3 K mol^{-1}, which are close to the theoretical value of 15.76 cm^3 K mol^{-1} for two isolated spin-only Gd(III) ions. Fig. 3 and S4, S5† display the perfect mirror-image CD spectra of these three enantiomeric pairs of ***R*/*S*-Eu**, ***R*/*S*-Gd** and ***R*/*S*-Eu-Ph$_3$PO** in CH_3OH with intense Cotton effects at 255 and 305 nm deriving from the equatorial macrocyclic Schiff-base, demonstrating their chiral nature. It should be noted that these macrocyclic compounds are stable up to 240 °C, as revealed by TGA analysis (Fig. S6 and S7†).

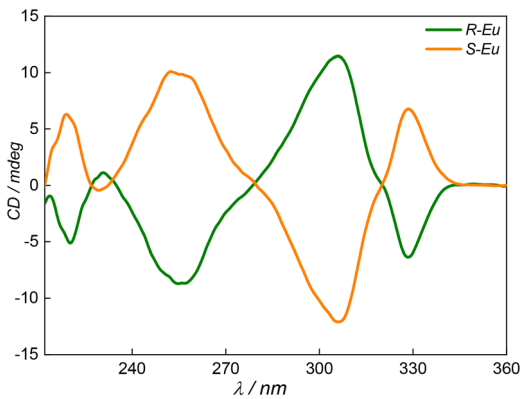

Fig. 3 CD spectra of ***R*/*S*-Eu** in CH_3OH (c = 1.0 × 10^{-5} mol L^{-1}).

Photophysical properties

The excitation and luminescence spectra of ***S*-Eu** were collected in CH_3OH solution at 1.0 × 10^{-5} mol L^{-1} at room temperature. Fig. 4 shows the excitation spectrum of ***S*-Eu** with a ligand-centered band between 275 and 350 nm when monitoring the transition $^5D_0 \rightarrow {}^7F_2$ of the Eu(III) ion at 617 nm. It can be clearly seen that two strong bands in the 275–350 nm range are located at the same wavelength in the absorption spectrum (Fig. 4 and S8†). The energy of the triplet state (T_1) located on the ligands was determined to be *ca.* 20 367 cm^{-1} by the zero-phonon component in the phosphorescence spectrum of the Gd(III) species (Fig. S8†). This value is 3117 cm^{-1} higher than the acceptance level of the Eu(III) ion. All these indicated efficient energy transfer from the ligand to the Eu(III) ion and

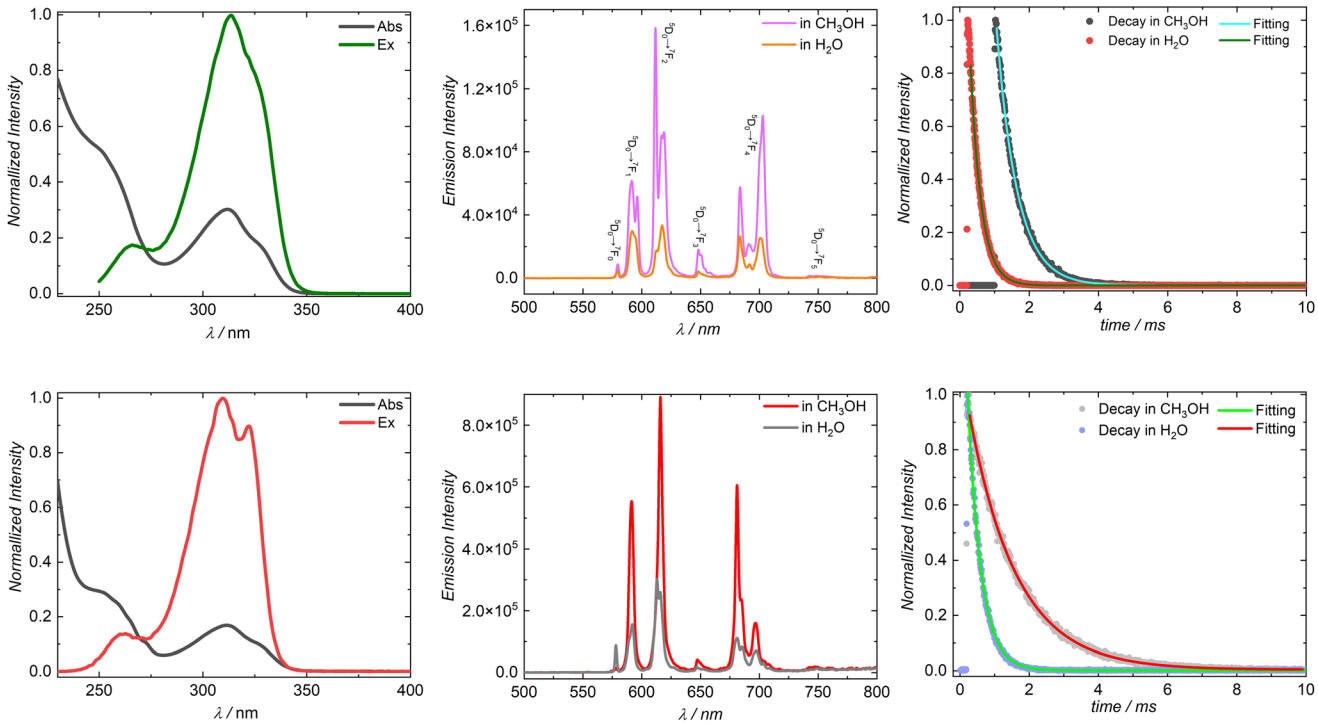

Fig. 4 Absorption and excitation spectra (left), emission spectra (middle) and decay curves (right) of ***S*-Eu** (top) and ***S*-Eu-Ph$_3$PO** (right) in CH_3OH and H_2O at room temperature, c = 1.0 × 10^{-5} mol L^{-1}.

suppressed back energy transfer from the Eu(III) ion to the ligand as the above energy gap is in the optimum range of 2000–5000 cm^{-1}.[8,39–41] Upon exciting the solution at 306 nm, all characteristic emission bands of the Eu(III) ion associated with $^5D_0 \rightarrow {}^7F_J$ (J = 0–5) transitions were clearly observed (Fig. 4). The spectrum was dominated by three bands which correspond to the transitions from the excited state $^5D_0$ to $^7F_1$ (591 nm), $^7F_2$ (612 nm), and $^7F_4$ (702 nm). In addition, it is evident that the emission intensities in H_2O are strongly weaker than those in CH_3OH, which can be expected because more O–H oscillators exist in the former that induce more serious nonradiative quenching processes. Quantum yields and luminescence lifetimes in both solutions were determined, up to 18.5% and 0.65 ms in CH_3OH and 7.2% and 0.33 ms in H_2O (Fig. S9 and S10†). As shown in Fig. 4, ***S*-Eu-Ph$_3$PO** showed similar optical properties and comparable quantum yields (Fig. S11 and S12†) to ***S*-Eu** but stronger emission intensity and longer luminescence lifetimes, *i.e.* 1.37 ms in CH_3OH and 0.38 ms in H_2O, under the same measurement conditions, as non-radiative quenching by O–H vibrations from coordinated water molecules in ***S*-Eu** was eradicated *via* replacing H_2O with Ph_3PO.

Circularly polarized luminescence spectra of two Eu(III) macrocycle enantiomers were also recorded in CH_3OH solution, which showed near-perfect mirror image signals (Fig. 5). It can be clearly seen that a strong CPL signal was observed at 597 nm, which is common for most chiral Eu(III) compounds and due to the special electronic and magnetic $^5D_0 \rightarrow {}^7F_1$ transitions.[23] The luminescence dissymmetry factor, g_{lum}, defined by $2(I_L - I_R)/(I_L + I_R)$ (where I_L and I_R are the emission intensities of left- and right-circularly polarized light, respectively), and B_{CPL}, were used to evaluate the CPL properties. As shown in Fig. S13 and S14† for the g_{lum} plots, ***S*-Eu-Ph$_3$PO** exhibited larger $|g_{lum}|$ values of the $^5D_0 \rightarrow {}^7F_1$ and $^5D_0 \rightarrow {}^7F_3$ transitions than ***S*-Eu**. The $|g_{lum}|$ values of the above two transitions of ***S*-Eu-Ph$_3$PO** increased by 10% compared to those of ***S*-Eu**, indicating that (i) the homochiral equatorial macrocycle is mainly responsible for the CPL activity; (ii) the replacement of solvent molecules enhances the molecular rigidity to some extent, therefore improving the CPL properties. The $|g_{lum}|$ values for the transition of $^5D_0 \rightarrow {}^7F_1$ are respectively 0.098 and 0.110 for ***S*-Eu** and ***S*-Eu-Ph$_3$PO**. The CPL brightness for these two compounds was also calculated and the median B_{CPL} values, 71.45 and 30.89 M^{-1} cm^{-1}, for the $^5D_0 \rightarrow {}^7F_1$ transition (λ_{exc} 329 nm, λ_{em} 597 nm) were obtained (Table S15†), which are comparable to Eu(PyBox)TTA$_3$,[42] CsEu(hfbc)$_4$ [43] and Eu(BnMeH22IAM).[44]

Relaxivity and *in vitro* MRI of Gd(III) chelates

Hydrophilic gadolinium(III) contrast agents, often affectionately called "gado" by medical workers,[45] have greatly expanded the utility of MRI which is a noninvasive clinical tool without ionizing radiation.[46,47] They can shorten the longitudinal relaxation time (T_1) of water protons in their vicinity by virtue of the slow electron relaxations and fast water exchange kinetics of gadolinium(III) ions in the S = 7/2 ground state, therefore affording brighter MR signals.[48] In the design of novel Gd(III)-based MR contrast agents (GBCAs), there have been several long recognized design principles (*vide infra*) at

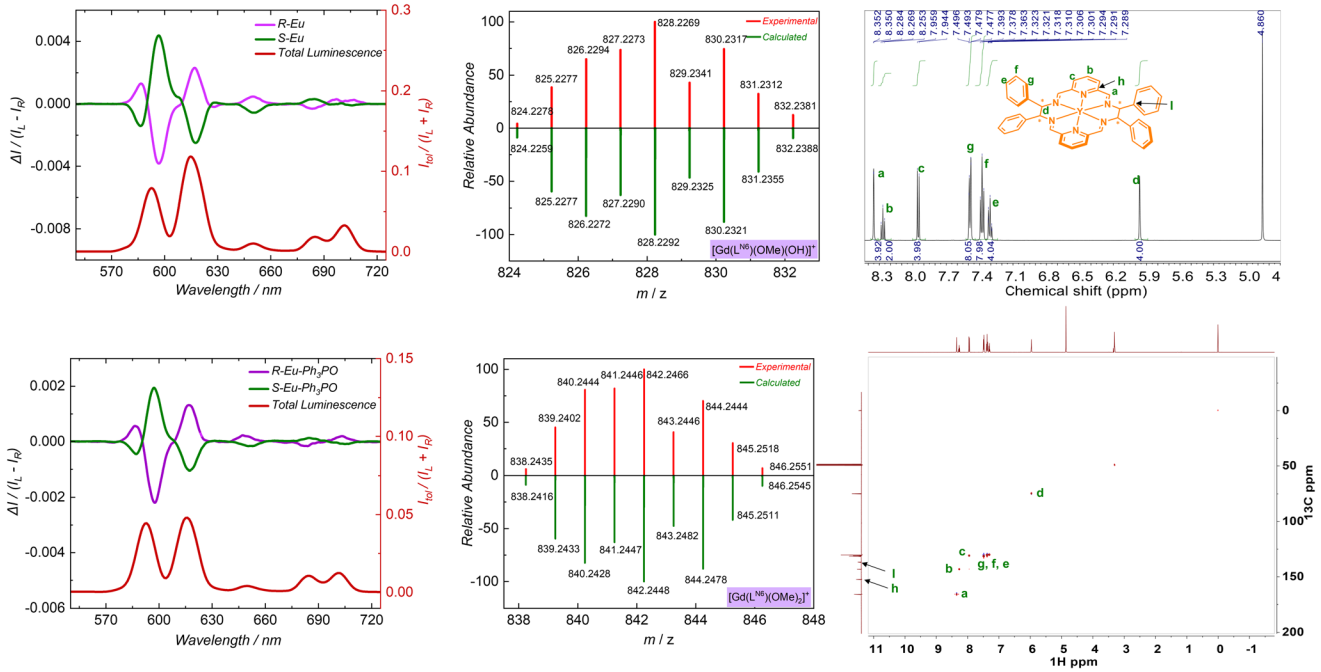

Fig. 5 (Left) CPL spectra and total luminescence traced in the background of ***R/S*-Eu** (top) and ***R/S*-Eu-Ph$_3$PO** (bottom) at room temperature in CH_3OH solution (c = 1.0 × 10^{-5} mol L^{-1}). Excitation at 329 nm. Bandpass: 10 nm; (middle) HR-ESI-MS of ***R/S*-Gd** in CH_3OH/H_2O solution, confirming the presence of the Gd(III) macrocycle; (right) ^{1}H NMR (top) and HMQC (bottom) of the diamagnetic Y(III) macrocycle, ***R*-Y**, in CD_3OD.

the molecular scale for high relaxivity (r_1), mainly involving three intrinsic physical parameters: the hydration number (q), the rotational correlation time (τ_R) and the water exchange rate ($1/\tau_m$).[49] Other molecular factors, *e.g.* electron relaxation and the Gd–H(water) distance (r_{Gd-H}), are usually not considered, as the former contributes little to r_1 in high magnetic fields while the latter is relatively difficult to control *via* chemical synthesis although it exhibits the inverse six power to T_{1m} (T_1 of the coordinated water molecule).[2] According to the following eqn (1)–(4), if a GBCA has q = 0, its relaxivity mainly comes from outer-sphere water molecules that are hydrogen bonded to the GBCA. Under this circumstance, polar groups will play a vital role in transmitting the relaxation.[50] For GBCAs with q > 0, the contribution of inner-sphere relaxation to r_1 should be considered. Theoretically, the greater the q value, the higher the inner-sphere relaxivity; however, more coordinated water molecules will greatly destroy the stability of chelates, increasing the risk of releasing toxic Gd(III) ions.[2,51] At present, almost all commercially approved GBCAs are macrocyclic chelates with a nine-coordinate Gd(III) ion and q = 1. For τ_R and τ_m, it should be noted that (i) τ_R dominates τ_c and further determines T_1; (ii) for small GBCAs, $\tau_m \ll T_{1m}$. Therefore, increasing r_1 can be achieved by slowing down the rotation of the compound. A straightforward and effective way is to increase the molecular weight of the compound by constructing a polynuclear structure or binding to macromolecules, *e.g.* serum albumin.[3,52,53]

As mentioned above, the Gd–O_{H_2O} distances are respectively 2.416(5) Å and 2.424(5) for ***S*-Gd** and ***R*-Gd** (Table S3†), which are shorter than the values in Gd-DOTA (2.463 Å) and Gd-DPTA (2.448 Å).[6,54,55] In addition, from the packing modes of solid structures shown in Fig. S4,† it was clearly observed that the Gd1-macrocycle interacts with the Gd2-macrocycle *via* an O–H···O–H···O–H···Cl hydrogen-bond bridge, forming a dimeric structure, and the coordinated water molecule also produces O–H···O–H hydrogen bonding interactions with two free CH_3OH molecules. The presence of abundant hydrogen bonds not only promotes second-sphere relaxation but also reduces the rate of molecular rotation.[2]

$$r_1 = r_1^{IS} + r_1^{OS} \quad (1)$$

$$r_1^{IS} = \frac{q/[H2O]}{T_{1m} + \tau_m} \quad (2)$$

$$T_{1m} = \frac{C}{r_{Gd-H}^6} \times \frac{3\tau_C}{1 + \omega_H{}^2\tau_C{}^2} (H > 0.1\,T) \quad (3)$$

$$\frac{1}{\tau_C} = \frac{1}{\tau_R} + \frac{1}{\tau_m} + \frac{1}{T_{1e}} \quad (4)$$

Where r_1^{IS} and r_1^{OS} are inner-sphere and outer-sphere relaxivity, respectively; C is a physical constant; τ_C is a correlation time for magnetic fluctuation and is composed of three parts: τ_R, the water residency time, τ_m and the electron relaxation time, T_{1e}.

One should be cautioned that although single-crystal X-ray diffraction confirmed the presence of a single aqua ligand that directly bonds to the Gd(III) ion (Fig. 3), the q value should be determined in solution by other physical methods, *e.g.* elec-

tron-nuclear double resonance spectroscopy and luminescence lifetime measurements of isostructural Eu(III) or Tb(III) complexes.[56,57] The luminescence lifetimes of the $^5D_0 \rightarrow {}^7F_2$ transition for the ***S*-Eu** complex in H_2O and D_2O are 0.33 ms and 1.7340 ms, respectively (Fig. 4 and S15†). Therefore, the hydration state for the Gd(III) complex was estimated from the equation proposed by Horrocks *et al.*[58] The obtained q value was 2.22, suggesting that the CH_3OH molecule coordinated to Gd2 was replaced by the water molecule.

The above structural characteristics imply a high r_1 for Gd(III) compounds. Before attempting the relaxivity rate characterization, the stability of ***R*/*S*-Ln** in solution was examined by NMR measurements. Given that the chemical shifts of paramagnetic lanthanide compounds span a wide range and are not even observed,[59] we prepared the analogous Yb(III) complex, ***R*-Y** (Tables S4 and S14†). As shown in Fig. 5, the ^1H and ^{13}C NMR spectra of ***R*-Y** in CD_3OD clearly showed 7 proton resonances and 9 carbon signals, indicating a single species with high symmetry in solution. Integration of the ^1H spectrum gives the formula of the species, $[Y(L^{N6})Cl_2]^+$. In addition, all ^1H and ^{13}C signals were accurately assigned combined with the HMQC spectrum. The HR-ESI-MS of ***S*-Gd** showed sharp peaks with +1 charge states, corresponding to Gd(III) macrocycles with different axial ligands (Fig. 5, middle). The MALDI-TOF-MS of the same compound exhibited one set of isotope peaks, indicating the species $[Gd(L^{N6})Cl_2]^+$ (Fig. S16†). The HR-ESI-MS spectrum of ***S*-Eu-Ph$_3$PO** and the ^1H spectrum of its isostructural Y(III) compound confirmed the presence of only one species of $[Eu(L^{N6})(Ph_3PO)_2(ClO_4)]^{2+}$ in solution (Fig. S17†), which is consistent with the solid structure determined by SCXRD. All results and analysis revealed that such macrocyclic compounds possess good solution stability. Fig. 6 and S18† illustrate the concentration-dependent behavior of the longitudinal relaxation rate ($1/T_1$) of Gd(III) compounds at 25 °C and 1.2 T. A linear fit of the data gives an r_1 value of 35.04 mM^{-1} s^{-1} for ***R*-Gd** and 34.09 mM^{-1} s^{-1} for ***S*-Gd**, respectively, *i.e.* each Gd(III) ion possesses a relatively high r_1, *ca.* 17 mM^{-1} s^{-1}. This value is much larger than that of commercially approved Gd(III)-based small molecules and comparable to that of some macromolecular compounds. In order to explore the potential of Gd(III)-based species in T_1-weighted MRI, we selected the commercially available Gd(III) MRI contrast agent, gadodiaminde hydrate, for comparison and first evaluated their cytotoxicities by the MTT assay. The results presented in Fig. S19† clearly show that the viabilities of A549 cells exceed 90% after incubation with various concentrations of ***R*/*S*-Gd** and gadodiaminde hydrate for 24 h, demonstrating that ***R*/*S*-Gd** do not exhibit obvious cell toxicity. Then, *in vitro* T_1-weighted MRI at 1.2 tesla was performed with A549 cells after incubation with the above three Gd(III) compounds for another 24 h and the results suggest that ***R*/*S*-Gd** possess comparable MR signal values to gadodiaminde hydrate (Fig. 6).

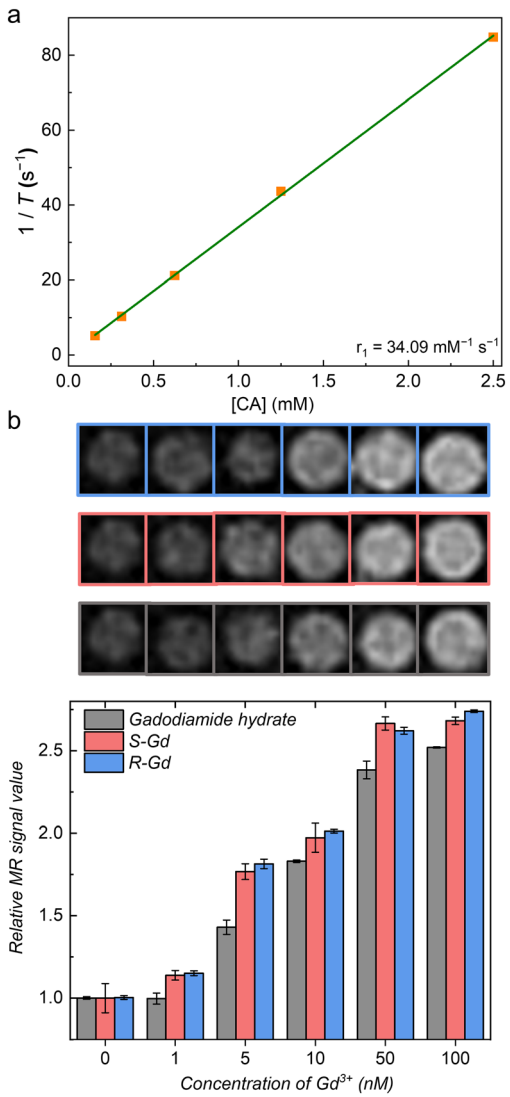

Fig. 6 (a) Relaxivity determined from concentration-dependent T_1-weighted MR measurements at 1.2 T (bottom) of ***S*-Gd** at room temperature; (b) T_1-weighted MRI of gadodiaminde hydrate (grey), ***S*-Gd** (soft red) and ***R*-Gd** (light blue) after incubation with A549 cells at various concentrations of Gd(III). The error bars mean the standard derivation (n = 3).

Conclusions

In conclusion, three pairs of mononuclear lanthanide macrocyclic enantiomers, ***R*/*S*-Eu**, ***R*/*S*-Gd** and ***R*/*S*-Eu-Ph$_3$PO**, were prepared *via* a facile [2 + 2] imine condensation with lanthanide ions as the template. Their enantiomeric relationship was verified by the mirror-symmetric solid structure determined from SCXRD and CD spectra. ***S*-Eu** exhibited brilliant photoluminescence and efficient CPL with an emission quantum yield, luminescence lifetime and luminescence dissymmetry factor of 18.5%, 0.65 ms and 0.098, respectively, in CH_3OH solution at room temperature, while isostructural Gd(III) chelates displayed one of the highest relaxivities to date, *ca.* 17 mM^{-1} s^{-1} per Gd(III) ion, low cell toxicity and efficient MRI at low concentrations. By employing Ph_3PO to replace H_2O and CH_3OH molecules located at the axial positions of ***S*-Eu**, a

longer luminescence lifetime was achieved in ***S*-Eu-Ph$_3$PO**, *i.e.* 1.37 ms in CH_3OH solution, benefitting from the eradication of non-radiative quenching by high energy O–H vibrations in the above solvent molecules. Biodistribution studies and *in vivo* MRI of Gd(III) species are underway.

Conflicts of interest

The authors declare no conflict of interest.

Acknowledgements

We thank the National Natural Science Foundation of China (22201279 and 22171100) for financial support.

References

1 W.-L. Zhou, Y. Chen, W. Lin and Y. Liu, Luminescent lanthanide–macrocycle supramolecular assembly, *Chem. Commun.*, 2021, **57**, 11443–11456.
2 J. Wahsner, E. M. Gale, A. Rodríguez-Rodríguez and P. Caravan, Chemistry of MRI Contrast Agents: Current Challenges and New Frontiers, *Chem. Rev.*, 2019, **119**, 957–1057.
3 A. J. L. Villaraza, A. Bumb and M. W. Brechbiel, Macromolecules, Dendrimers, and Nanomaterials in Magnetic Resonance Imaging: The Interplay between Size, Function, and Pharmacokinetics, *Chem. Rev.*, 2010, **110**, 2921–2959.
4 G.-Q. Jin, C. V. Chau, J. F. Arambula, S. Gao, J. L. Sessler and J.-L. Zhang, Lanthanide porphyrinoids as molecular theranostics, *Chem. Soc. Rev.*, 2022, **51**, 6177–6209.
5 R. Jankowski, M. Wyczesany and S. Chorazy, Multifunctionality of luminescent molecular nanomagnets based on lanthanide complexes, *Chem. Commun.*, 2023, **59**, 5961–5986.
6 C. A. Chang, L. C. Francesconi, M. F. Malley, K. Kumar, J. Z. Gougoutas, M. F. Tweedle, D. W. Lee and L. J. Wilson, Synthesis, characterization, and crystal structures of M(DO_3A) (M = iron, gadolinium) and Na[M(DOTA)] (M = Fe, yttrium, Gd), *Inorg. Chem.*, 1993, **32**, 3501–3508.
7 J.-Y. Hu, Y. Ning, Y.-S. Meng, J. Zhang, Z.-Y. Wu, S. Gao and J.-L. Zhang, Highly near-IR emissive ytterbium(III) complexes with unprecedented quantum yields, *Chem. Sci.*, 2017, **8**, 2702–2709.
8 J.-X. Zhang, W.-L. Chan, C. Xie, Y. Zhou, H.-F. Chau, P. Maity, G. T. Harrison, A. Amassian, O. F. Mohammed, P. A. Tanner, W.-K. Wong and K.-L. Wong, Impressive near-infrared brightness and singlet oxygen generation from strategic lanthanide–porphyrin double-decker complexes in aqueous solution, *Light: Sci. Appl.*, 2019, **8**, 46.
9 N. Ishikawa, M. Sugita, T. Ishikawa, S.-Y. Koshihara and Y. Kaizu, Lanthanide Double-Decker Complexes Functioning as Magnets at the Single-Molecular Level, *J. Am. Chem. Soc.*, 2003, **125**, 8694–8695.
10 H. Wada, S. Ooka, T. Yamamura and T. Kajiwara, Light Lanthanide Complexes with Crown Ether and Its Aza Derivative Which Show Slow Magnetic Relaxation Behaviors, *Inorg. Chem.*, 2017, **56**, 147–155.
11 W. Radecka-Paryzek, Template synthesis and characterization of 18-membered hexaaza macrocyclic complex of lanthanum(III) perchlorate, *Inorg. Chim. Acta*, 1980, **45**, L147–L148.
12 S. Akine, S. Sunaga, T. Taniguchi, H. Miyazaki and T. Nabeshima, Core/Shell Oligometallic Template Synthesis of Macrocyclic Hexaoxime, *Inorg. Chem.*, 2007, **46**, 2959–2961.
13 R. K. Das, E. Barnea, T. Andrea, M. Kapon, N. Fridman, M. Botoshansky and M. S. Eisen, Group 4 Lanthanide and Actinide Organometallic Inclusion Complexes, *Organometallics*, 2015, **34**, 742–752.
14 J. Long, J. Rouquette, J.-M. Thibaud, R. A. S. Ferreira, L. D. Carlos, B. Donnadieu, V. Vieru, L. F. Chibotaru, L. Konczewicz, J. Haines, Y. Guari and J. Larionova, A High-Temperature Molecular Ferroelectric Zn/Dy Complex Exhibiting Single-Ion-Magnet Behavior and Lanthanide Luminescence, *Angew. Chem., Int. Ed.*, 2015, **54**, 2236–2240.
15 J. Long, M. S. Ivanov, V. A. Khomchenko, E. Mamontova, J.-M. Thibaud, J. Rouquette, M. Beaudhuin, D. Granier, R. A. S. Ferreira, L. D. Carlos, B. Donnadieu, M. S. C. Henriques, J. A. Paixão, Y. Guari and J. Larionova, Room temperature magnetoelectric coupling in a molecular ferroelectric ytterbium(III) complex, *Science*, 2020, **367**, 671–676.
16 L. Dai, C. M. Jones, W. T. K. Chan, T. A. Pham, X. Ling, E. M. Gale, N. J. Rotile, W. C.-S. Tai, C. J. Anderson, P. Caravan and G.-L. Law, Chiral DOTA chelators as an improved platform for biomedical imaging and therapy applications, *Nat. Commun.*, 2018, **9**, 857.
17 J. M. Van Raden, D. I. Alexandropoulos, M. Slota, S. Sopp, T. Matsuno, A. L. Thompson, H. Isobe, H. L. Anderson and L. Bogani, Singly and Triply Linked Magnetic Porphyrin Lanthanide Arrays, *J. Am. Chem. Soc.*, 2022, **144**, 8693–8706.
18 K. Wang, F. Ma, D. Qi, X. Chen, Y. Chen, Y.-C. Chen, H.-L. Sun, M.-L. Tong and J. Jiang, Chiral bis(phthalocyaninato) terbium double-decker compounds with enhanced single-ion magnetic behavior, *Inorg. Chem. Front.*, 2018, **5**, 939–943.
19 C. Zhao, Z. Zhu, X.-L. Li and J. Tang, Air-stable chiral mono- and dinuclear dysprosium single-molecule magnets: steric hindrance of hexaazamacrocycles, *Inorg. Chem. Front.*, 2022, **9**, 4049–4055.
20 T. Morita, M. Damjanović, K. Katoh, Y. Kitagawa, N. Yasuda, Y. Lan, W. Wernsdorfer, B. K. Breedlove, M. Enders and M. Yamashita, Comparison of the Magnetic Anisotropy and Spin Relaxation Phenomenon of Dinuclear Terbium(III) Phthalocyaninato Single-Molecule Magnets Using the Geometric Spin Arrangement, *J. Am. Chem. Soc.*, 2018, **140**, 2995–3007.

21 H.-Y. Wong, W.-S. Lo, K.-H. Yim and G.-L. Law, Chirality and Chiroptics of Lanthanide Molecular and Supramolecular Assemblies, *Chem*, 2019, **5**, 3058–3095.
22 R. Carr, N. H. Evans and D. Parker, Lanthanide complexes as chiral probes exploiting circularly polarized luminescence, *Chem. Soc. Rev.*, 2012, **41**, 7673–7686.
23 L. Arrico, L. Di Bari and F. Zinna, Quantifying the Overall Efficiency of Circularly Polarized Emitters, *Chem. – Eur. J.*, 2021, **27**, 2920–2934.
24 J. L. Lunkley, D. Shirotani, K. Yamanari, S. Kaizaki and G. Muller, Extraordinary Circularly Polarized Luminescence Activity Exhibited by Cesium Tetrakis(3-heptafluoro-butylryl-(+)-camphorato) Eu(III) Complexes in EtOH and $CHCl_3$ Solutions, *J. Am. Chem. Soc.*, 2008, **130**, 13814–13815.
25 M. C. Heffern, L. M. Matosziuk and T. J. Meade, Lanthanide Probes for Bioresponsive Imaging, *Chem. Rev.*, 2014, **114**, 4496–4539.
26 N. F. M. Mukthar, N. D. Schley and G. Ung, Strong Circularly Polarized Luminescence at 1550 nm from Enantiopure Molecular Erbium Complexes, *J. Am. Chem. Soc.*, 2022, **144**, 6148–6153.
27 B.-A. N. Willis, D. Schnable, N. D. Schley and G. Ung, Spinolate Lanthanide Complexes for High Circularly Polarized Luminescence Metrics in the Visible and Near-Infrared, *J. Am. Chem. Soc.*, 2022, **144**, 22421–22425.
28 J. Zhang, L. Dai, A. M. Webster, W. T. K. Chan, L. E. Mackenzie, R. Pal, S. L. Cobb and G.-L. Law, Unusual Magnetic Field Responsive Circularly Polarized Luminescence Probes with Highly Emissive Chiral Europium(III) Complexes, *Angew. Chem., Int. Ed.*, 2021, **60**, 1004–1010.
29 W. Radecka-Paryzek, V. Patroniak and M. Kubicki, The template synthesis and characterization of pentaaza macrocyclic complexes of rare earth elements. The crystal structure of the 2,14-dimethyl-3,6,10,13,19-pentaazabicyclo [13.3.1]nonadeca-1(19),2,13,15,17-pentaene-dichlorolutetium(III)perchlorate, *Polyhedron*, 2003, **22**, 2773–2779.
30 Y. Gil, A. Castro-Alvarez, P. Fuentealba, E. Spodine and D. Aravena, Lanthanide SMMs Based on Belt Macrocycles: Recent Advances and General Trends, *Chem. – Eur. J.*, 2022, **28**, e202200336.
31 Z. Zhu, C. Zhao, T. Feng, X. Liu, X. Ying, X.-L. Li, Y.-Q. Zhang and J. Tang, Air-Stable Chiral Single-Molecule Magnets with Record Anisotropy Barrier Exceeding 1800 K, *J. Am. Chem. Soc.*, 2021, **143**, 10077–10082.
32 M. Wasim, K. U. Ansari, P. Kumar, B. Mallick and M. Shanmugam, A unique and discrete Ce(III) macrocyclic complex exhibits ferroelectric, dielectric, and slow relaxation of magnetization properties, *Inorg. Chem. Front.*, 2022, **9**, 2284–2289.
33 Z. Zhu, G.-Q. Jin, J. Wu, X. Ying, C. Zhao, J.-L. Zhang and J. Tang, Highly symmetric Ln(III) boron-containing macrocycles as bright fluorophores for living cell imaging, *Inorg. Chem. Front.*, 2022, **9**, 5048–5054.
34 F. Hamon, E. Largy, A. Guédin-Beaurepaire, M. Rouchon-Dagois, A. Sidibe, D. Monchaud, J.-L. Mergny, J.-F. Riou, C.-H. Nguyen and M.-P. Teulade-Fichou, An Acyclic Oligoheteroaryle That Discriminates Strongly between Diverse G-Quadruplex Topologies, *Angew. Chem., Int. Ed.*, 2011, **50**, 8745–8749.
35 O. V. Dolomanov, L. J. Bourhis, R. J. Gildea, J. A. K. Howard and H. Puschmann, OLEX2: a complete structure solution, refinement and analysis program, *J. Appl. Crystallogr.*, 2009, **42**, 339–341.
36 G. Sheldrick, SHELXT - Integrated space-group and crystal-structure determination, *Acta Crystallogr., Sect. A: Found. Adv.*, 2015, **71**, 3–8.
37 G. Sheldrick, Crystal structure refinement with SHELXL, *Acta Crystallogr., Sect. C: Struct. Chem.*, 2015, **71**, 3–8.
38 S. Biju, N. Gopakumar, J. C. G. Bünzli, R. Scopelliti, H. K. Kim and M. L. P. Reddy, Brilliant Photoluminescence and Triboluminescence from Ternary Complexes of Dy^{III} and Tb^{III} with 3-Phenyl-4-propanoyl-5-isoxazolonate and a Bidentate Phosphine Oxide Coligand, *Inorg. Chem.*, 2013, **52**, 8750–8758.
39 J.-C. G. Bünzli, On the design of highly luminescent lanthanide complexes, *Coord. Chem. Rev.*, 2015, **293–294**, 19–47.
40 O. L. Malta, Mechanisms of non-radiative energy transfer involving lanthanide ions revisited, *J. Non-Cryst. Solids*, 2008, **354**, 4770–4776.
41 T. N. Nguyen, C. Y. Chow, S. V. Eliseeva, E. R. Trivedi, J. W. Kampf, I. Martinić, S. Petoud and V. L. Pecoraro, One-Step Assembly of Visible and Near-Infrared Emitting Metallacrown Dimers Using a Bifunctional Linker, *Chem. – Eur. J.*, 2018, **24**, 1031–1035.
42 M. Górecki, L. Carpita, L. Arrico, F. Zinna and L. Di Bari, Chiroptical methods in a wide wavelength range for obtaining Ln^{3+} complexes with circularly polarized luminescence of practical interest, *Dalton Trans.*, 2018, **47**, 7166–7177.
43 F. Zinna, U. Giovanella and L. D. Bari, Highly Circularly Polarized Electroluminescence from a Chiral Europium Complex, *Adv. Mater.*, 2015, **27**, 1791–1795.
44 S. Petoud, G. Muller, E. G. Moore, J. Xu, J. Sokolnicki, J. P. Riehl, U. N. Le, S. M. Cohen and K. N. Raymond, Brilliant Sm, Eu, Tb, and Dy Chiral Lanthanide Complexes with Strong Circularly Polarized Luminescence, *J. Am. Chem. Soc.*, 2007, **129**, 77–83.
45 P. Caravan, J. J. Ellison, T. J. McMurry and R. B. Lauffer, Gadolinium(III) Chelates as MRI Contrast Agents: Structure, Dynamics, and Applications, *Chem. Rev.*, 1999, **99**, 2293–2352.
46 J.-H. Tang, H. Li, C. Yuan, G. Parigi, C. Luchinat and T. J. Meade, Molecular Engineering of Self-Immolative Bioresponsive MR Probes, *J. Am. Chem. Soc.*, 2023, **145**, 10045–10050.
47 P. Caravan, Protein-Targeted Gadolinium-Based Magnetic Resonance Imaging (MRI) Contrast Agents: Design and Mechanism of Action, *Acc. Chem. Res.*, 2009, **42**, 851–862.
48 E. M. Gale, I. P. Atanasova, F. Blasi, I. Ay and P. Caravan, A Manganese Alternative to Gadolinium for MRI Contrast, *J. Am. Chem. Soc.*, 2015, **137**, 15548–15557.
49 H. Li and T. J. Meade, Molecular Magnetic Resonance Imaging with Gd(III)-Based Contrast Agents: Challenges

and Key Advances, *J. Am. Chem. Soc.*, 2019, **141**, 17025–17041.

50 G.-Q. Jin, H. Lai, Z.-S. Yang, Y. Ning, L. Duan, J. Zhang, T. Chen, S. Gao and J.-L. Zhang, Gadolinium(III) Porphyrinoid Phototheranostics, *Chem. – Asian J.*, 2022, **17**, e202200181.

51 M. Polasek and P. Caravan, Is Macrocycle a Synonym for Kinetic Inertness in Gd(III) Complexes? Effect of Coordinating and Noncoordinating Substituents on Inertness and Relaxivity of Gd(III) Chelates with DO3A-like Ligands, *Inorg. Chem.*, 2013, **52**, 4084–4096.

52 Z. Wang, L. He, B. Liu, L.-P. Zhou, L.-X. Cai, S.-J. Hu, X.-Z. Li, Z. Li, T. Chen, X. Li and Q.-F. Sun, Coordination-Assembled Water-Soluble Anionic Lanthanide Organic Polyhedra for Luminescent Labeling and Magnetic Resonance Imaging, *J. Am. Chem. Soc.*, 2020, **142**, 16409–16419.

53 Z. Zhang, M. T. Greenfield, M. Spiller, T. J. McMurry, R. B. Lauffer and P. Caravan, Multilocus Binding Increases the Relaxivity of Protein-Bound MRI Contrast Agents, *Angew. Chem., Int. Ed.*, 2005, **44**, 6766–6769.

54 M. Briganti, E. Lucaccini, L. Chelazzi, S. Ciattini, L. Sorace, R. Sessoli, F. Totti and M. Perfetti, Magnetic Anisotropy Trends along a Full 4f-Series: The f^{n+7} Effect, *J. Am. Chem. Soc.*, 2021, **143**, 8108–8115.

55 S. Gao, S. J. George and Z.-H. Zhou, Interaction of Gd-DTPA with phosphate and phosphite: toward the reaction intermediate in nephrogenic systemic fibrosis, *Dalton Trans.*, 2016, **45**, 5388–5394.

56 S. G. Zech, W.-C. Sun, V. Jacques, P. Caravan, A. V. Astashkin and A. M. Raitsimring, Probing the Water Coordination of Protein-Targeted MRI Contrast Agents by Pulsed ENDOR Spectroscopy, *ChemPhysChem*, 2005, **6**, 2570–2577.

57 W. D. Horrocks Jr. and D. R. Sudnick, Lanthanide ion probes of structure in biology. Laser-induced luminescence decay constants provide a direct measure of the number of metal-coordinated water molecules, *J. Am. Chem. Soc.*, 1979, **101**, 334–340.

58 R. M. Supkowski and W. D. Horrocks, On the determination of the number of water molecules, q, coordinated to europium(III) ions in solution from luminescence decay lifetimes, *Inorg. Chim. Acta*, 2002, **340**, 44–48.

59 A. Gerus, K. Ślepokura and J. Lisowski, Anion and Solvent Induced Chirality Inversion in Macrocyclic Lanthanide Complexes, *Inorg. Chem.*, 2013, **52**, 12450–12460.